Proceedings 10th NUMGE 2023
10th European Conference on Numerical Methods in Geotechnical Engineering
Zdravkovic L, Kontoe S, Taborda DMG, Tsiampousi A (eds)

https://doi.org/10.53243/NUMGE2023-131

Undrained uplift capacity of single helical piles and helical pile groups

N. Stefopoulos[1], K. Georgiadis[2], T. Nikolaidis[3]

[1,2,3]*Department of Civil Engineering, Aristotle University of Thessaloniki, Thessaloniki, Greece*

ABSTRACT: Recent studies have examined the use of single helical piles as anchors for offshore wind turbines and have identified problems related to the necessary upscaling of such piles to meet the high required uplift capacity. An alternative attractive foundation solution that has been proposed to overcome these problems is to use groups of helical piles instead of single piles. In this paper the uplift capacity of individual helices, helical piles and helical pile groups, in undrained clay, is examined using three-dimensional finite element analyses. The results are first validated through comparison with existing numerical and analytical solutions for circular plates. Subsequently, three-dimensional analyses are presented in which individual helices are loaded to failure and shape effects on the bearing capacity and on the associated failure mechanisms are investigated. The effect of factors such as helix-soil adhesion and helix pitch on the bearing capacity is also examined. Finally, helical pile group analyses are presented, in which four-pile and sixteen-pile group layouts with several axial pile spacings are considered.

Keywords: helical piles; bearing capacity; clays; finite-element modelling; wind turbines

1 INTRODUCTION

Helical piles have been widely used in onshore applications (Perko, 1995). Recently they have been proposed as anchors for offshore wind turbines (Byrne and Houlsby, 2015; Castro-Santos and Diaz-Casas, 2016; Spagnoli, 2013) due to their easy installation, their sustainable characteristics, in terms of produced installation noise (Houlsby, 2016), and due to their potential reusability. Hence, they have been characterized as a green foundation system (Ullah et al., 2019).

But to meet the increased uplift capacity problems, due to the extreme prevailing conditions that occur in the offshore environment, new helical piles of increased dimensions need to be developed. However, the upscaling comes with structural integrity issues and the need for development of new torque devices. Thus, the use of groups of helical piles has been proposed, as an innovative solution that could possibly address these problems (Elsherbiny, 2011; Lanyi-Bennett and Deng, 2017).

This paper presents a numerical investigation of the ultimate uplift capacity of single helices, helical piles, a four- and a sixteen-pile group in clay. In all cases, the helices are located at sufficient depth to eliminate the effect of the ground surface, therefore, only the development of deep failure mechanisms is considered.

Since limited work has been published for the case of helical pile groups, group effects are investigated and quantified herein. Specifically, the effect of the axial spacing on the total group capacity is examined.

It is important to mention that in this paper the helices are not idealized, as done conventionally, as plates. The actual geometry is modelled using three-dimensional analyses and shape effects are examined.

2 FINITE ELEMENT ANALYSES

The displacement finite-element analyses presented in this paper were performed using the finite element programs PLAXIS 2D and 3D. Several finite element meshes are used in the analyses; for a single helix, a single helical pile and for helical pile groups of various axial spacings.

In all cases, the piles are buried in undrained clay, which is modelled as an elastic – perfectly plastic Tresca material with Poisson's ratio ν = 0.495, undrained Young's modulus E = 20 MPa, and undrained shear strength s_u = 50 kPa. The helix and shaft of the helical piles is modelled as linear elastic with steel properties: Young's modulus E = 210 GPa and Poisson's ratio ν = 0.1. The soil-plate interaction is modelled using interface elements with either zero adhesion (perfectly smooth interface) or full adhesion (perfectly rough interface).

Regarding the steel structure dimensions, the shaft is modelled as a tube with a radius of R=0.1 m and a total length of L=7.0m. The helix has a radius of R_0=0.5 m and the pitch varies from p=0.30 to 0.50 m. Both the helices and the shaft thicknesses are equal to t=0.02 m. Note that the rigidity of the structures is secured by applying uniform displacement to both structures.

A typical three-dimensional finite element mesh is shown in Figure 1. Mesh dimensions vary from 3m x 3m

x 3m (width x depth x height) to 6.5m x 6.5m x 7m (width x depth x height) for different model configurations and are selected such as to not affect the failure mechanism but also reduce the computational time. To accurately model the helix geometry and to obtain accurate failure loads, large numbers of elements are used. The soil is modelled with approximately 340.000 to 495.000 10-noded, tetrahedral elements, the helices with 2.900 6-node plate elements each, while the soil-structure interaction using 12-node interface elements. The vertical boundaries are fixed in the normal direction while the bottom boundary is fully fixed.

The two-dimensional mesh is cylindrical and is modelled making use of the axial symmetry of the geometry, as a 10m x 10m rectangular surface, with the exact same soil and structure properties as in the 3D analyses, and approximately 5000 15-node triangular soil elements and about 600 triangular 6-node plate elements. Finally, 12-node interface elements were used between the pile and the soil.

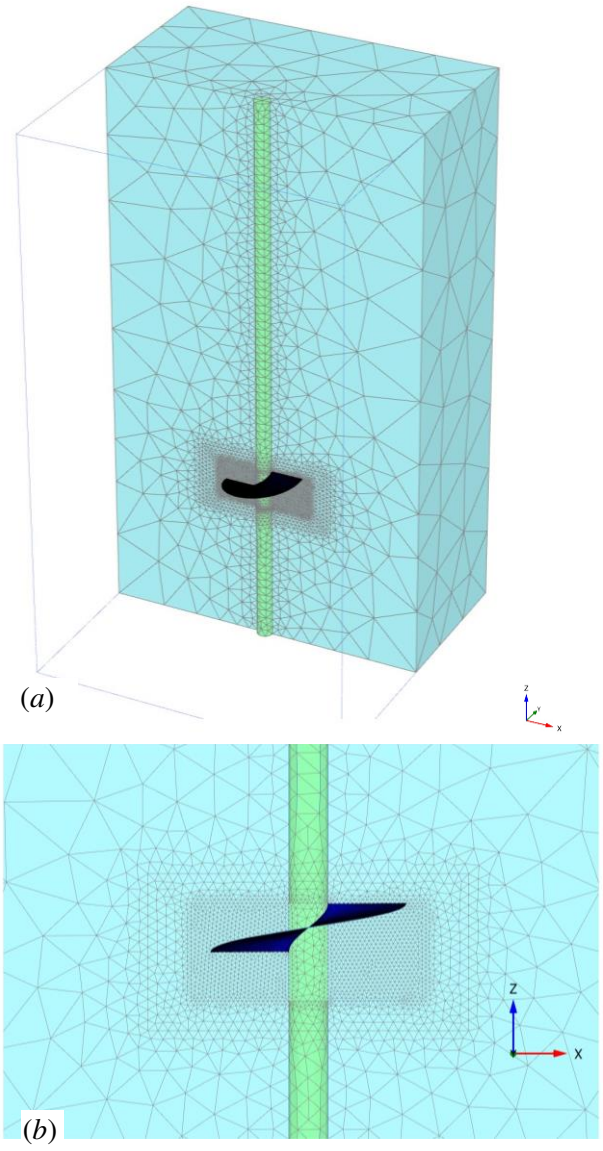

Figure 1. Single helical pile three-dimensional mesh (a) Half-mesh (b) detail of mesh refinement

3 VERIFICATION

3.1 2D finite element analyses

Zhao et al. (2015) approximated the helix geometry as an axisymmetric tapered plate and developed an analytical upper bound plasticity solution for a single tapered plate anchor buried deeply in uniform clay. They also proposed the following equation to correlate the tapered plate angle β_p with the helix pitch p:

$$\beta_p = \arctan\left(\frac{p}{2R_0}\right) \quad (1)$$

To verify the validity of the numerical study presented here, axisymmetric analyses of tapered plates were first performed, and the results were compared to those by Zhao et al. (2015). The results are compared in terms of the uplift capacity factor, which is defined through the following equation:

$$N_c = \frac{F}{\pi R_0^2 \, s_u} \quad (2)$$

where F is the ultimate axial load.

A comparison of the calculated undrained bearing capacity factors is presented in Tables 1 and 2, for smooth and rough soil-plate interfaces, respectively. As seen in these tables, the numerical and upper bound results compare well (maximum difference of 2.25%) for both smooth and rough interfaces. In the case of a smooth interface the numerical results always slightly overestimate bearing capacity compared with the upper bound solution, while the opposite is true in the case of a rough interface.

Table 1. Comparison of bearing capacity factors for smooth plate-soil interface

β_p	N_c^{FE}	N_c^{Zhao}	Difference
10.00	11.913	11.650	2.3%
16.69	11.544	11.383	1.4%
20.00	11.438	11.220	1.9%

Table 2. Comparison of bearing capacity factors for rough plate-soil interface

β_p	N_c^{FE}	N_c^{Zhao}	Difference
10.00	12.824	12.930	-0.8%
16.69	12.794	12.930	-1.1%
20.00	12.781	12.930	-1.2%

3.2 3D finite element analyses

To verify the validity of the three-dimensional finite element modelling procedure, both two- and three- dimensional FE analyses of a circular disc with a radius of R_0 =0.50 m were performed with PLAXIS 2D and 3D. The calculated uplift bearing capacity factors are compared

in Table 3. Good agreement is observed between 2D and 3D FEA; the differences between them are 3.8% and 3% for smooth (adhesion factor α = 0) and rough (adhesion factor α = 1) plate-soil interfaces respectively, with the three-dimensional analyses always slightly overestimating the bearing capacity.

Table 3. Comparison of bearing capacity factors for a circular disc against

a	$N_c^{FE,2D}$	$N_c^{FE,3D}$	Difference
0.0	13.002	13.497	3.8%
1.0	13.515	13.919	3%

A further comparison of the three-dimensional FE bearing capacity factors is made with those obtained by Martin and Randolph (2001) and Merifield (2011) in Table 4. As seen, the results are also in relatively good agreement for both smooth and rough plate-soil interfaces.

Table 4. Comparison of bearing capacity factors for a circular disc.

a	N_c^{Martin}	$N_c^{Merifield}$	$N_c^{FE,3D}$	Difference
0.0	12.640	12.560	13.497	6.8%
1.0	13.310	N/A	13.919	4.6%

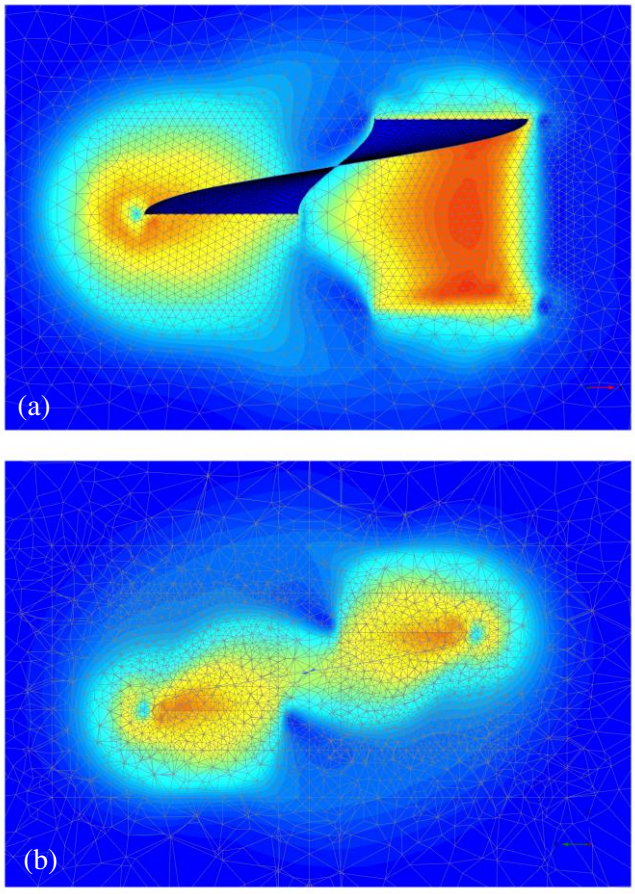

Figure 2. Failure mechanism of a smooth helix (a) on the xz plane (b) on the yz plane.

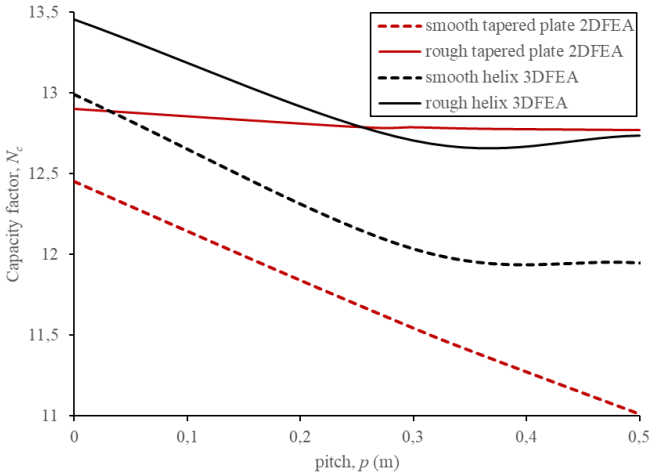

Figure 3. Effect of helix pitch on the capacity factor for helices and tapered plates.

4 SINGLE HELICAL PILES

A series of displacement finite element analyses were performed to investigate the effect of parameters such as the helix geometry, the adhesion factor, and the shaft on the bearing capacity of single helical piles.

4.1 Effect of helix geometry

Figure 2 presents the failure mechanism for a smooth helix with the following dimensions: R_0=0.5 m and p=0.5 m. As expected, the failure mechanism is different compared to the axisymmetric failure mechanisms for discs and tapered plates. As illustrated in Figure 2, part of the mechanism, on the side that the helix does not overlap, forms the characteristic bulb shape, similar to the axisymmetric disc and tapered plate failure mechanisms, but the rest of the mechanism on the overlapping area shows that the soil moves vertically and uniformly as a rigid body along with the helix.

The uplift capacity factors, N_c, for a disc, a tapered plate and a helix are presented in Tables 5 and 6, for perfectly smooth (α = 0) or rough (α = 1) interfaces, respectively. It can be observed that for both smooth and rough interfaces, the idealization of a helix as a disc results in an overestimation of the uplift capacity factor. This overestimation is between 8% and 9% for the cases considered in this study.

Approximating the helix as a tapered plate, using Equation 1 to determine the equivalent taper angle β_p, results in an underestimation of N_c, in the case of a smooth interface, of 4% to 7% and a very small overestimation of less than 1.5% for rough interfaces.

The effect of the pitch is illustrated in Figure 3, which shows the variation of the uplift capacity factor with the helix pitch for smooth and rough helices. As seen in this figure, N_c decreases as the helix pitch increases from 0 to 0.30 m and remains relatively constant for greater pitch values. Also shown in Figure 3 is the variation of N_c for tapered plates, obtained from two-dimensional

analyses, in which the equivalent pitch is determined through Equation (1). The effect of the pitch is different in this case. In contrast to what is observed for helices, the pitch has practically no effect when the tapered plate is rough, while N_c continuously decreases with the increase of the pitch for smooth plates.

Table 5. Comparison of capacity factors for smooth plate-soil interfaces. (a=0)

$p\ (m)$	N_c^{disc}	$N_c^{tapered}$	N_c^{helix}
0.30	12.99	11.54	12.032
0.50	12.99	11.09	11.945

Table 6. Comparison of capacity factors for rough plate-soil interfaces. (a=1)

$p\ (m)$	N_c^{disc}	$N_c^{tapered}$	N_c^{helix}
0.30	13.46	12.93	12.707
0.50	13.46	12.93	12.738

4.2 Effect of the pile shaft

To investigate the effect of the pile shaft on the uplift capacity of a helix, 3D analyses were performed in which a rigid shaft with radius $R = 0.10$m was modelled. In all cases the shaft was perfectly smooth, in order to isolate the contribution of the helix to the overall capacity. The finite element analyses results for these cases are presented in the form of a modified uplift capacity factor, N_c^*, that is defined in Equation (3):

$$N_c^* = \frac{F}{\pi\left(R_0^2 - R^2\right) s_u} \tag{3}$$

Table 7 shows that the pile shaft does not have a significant effect on the calculated uplift capacity of the helix. In all cases, the difference between the modified uplift capacity factor of a helix with a shaft and the uplift capacity factor of the same helix without a shaft is less than 3%.

Table 7. Comparison of uplift capacity factors of helical piles and helices.

a	p (m)	$N_{c,hel.pile}^*$	N_c^{helix}
0.0	0.30	12.043	12.032
	0.50	11.798	11.945
1.0	0.30	13.045	12.707
	0.50	12.922	12.738

4.3 Effect of helix-soil adhesion

As seen in Figure 3, the effect of adhesion is greater for tapered plates than for helices. For tapered plates, the difference between the uplift capacity factors for rough and smooth plates increases with the increase of the equivalent helix pitch and reaches 16% (greater capacity for a rough compared to a smooth plate) when the pitch is equal to 0.5m. The effect of adhesion on the uplift capacity of helices is smaller. The capacity factor of a rough helix is only up to 6.5% greater than that of a smooth helix in the cases considered in this study. However, when the pile shaft is also modelled, adhesion becomes more important. As seen in Table 7, helical piles with a rough helix-soil interface have 10% greater uplift capacity than helical piles with smooth helix-soil interfaces for a pitch equal to $0.50\ m$.

5 HELICAL PILE GROUPS

Three-dimensional FE analyses of a 2x2 and a 4x4 helical pile group were performed in order to investigate group effects. Several axial pile spacings were considered: s/D_{helix} = 1.1, 1.2, 1.4, 1.6, 2.0. The dimensions of the helices are the following: p=0.5 m, R=0.1 m, R_0=0.5 m, t=0.02 m. Only the case of perfectly rough interface is considered. Group effects are quantified in terms of the pile group effectiveness, n, which is defined as the ratio of the pile group ultimate uplift capacity over the sum of the individual single pile capacities. In all cases, the pile shafts are perfectly smooth. Taking advantage of the symmetry of the helical pile group and in order to reduce the computational time, only a quarter of the problem was analysed.

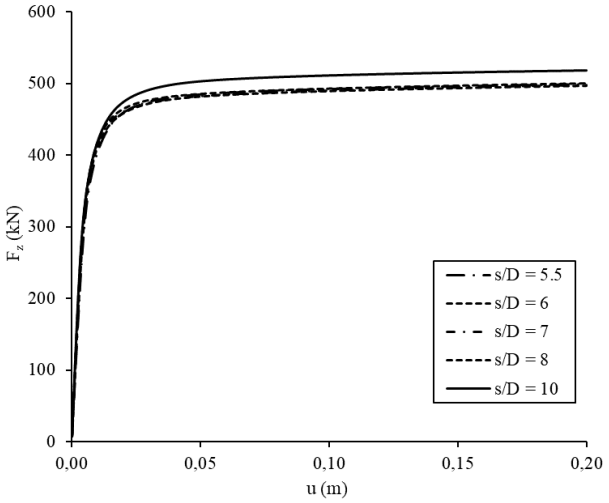

Figure 4. Load-displacement diagram for a 2x2 helical pile group.

5.1 Group of 4 helical piles

Figure 4 presents the axial load-displacement curves for one of the four identical piles of a 2x2 helical pile group. It can be seen in this figure that the curves have reached a plateau at an axial displacement of 0.20 m, i.e. at 20% of the helix diameter.

The variation of the calculated pile group efficiency n with the normalised pile spacing s/D_{shaft} is illustrated in Figure 5. The obtained values of n are also presented together with calculated uplift capacities in Table 8. It can be seen that as the pile spacing increases, group

effectiveness initially decreases, reaching the minimum value of 0.95 at s/D_{helix}=1.2 or s/D_{shaft}=6, and then gradually increases and approaches the limiting value of 1, that corresponds to zero group effects, at s/D_{helix} =2 or s/D_{shaft} =10. The failure mechanism for s/D_{helix} =1.2 is presented in Figure 6. As seen, it extends to the plane of symmetry, and therefore it effectively overlaps with the failure mechanism of the adjacent pile.

Additional analyses performed to investigate potential effects of the orientation of the helices with respect to the plane of symmetry showed that the influence is negligible.

Table 8. Group capacity factors and bearing capacity in relation to the axial distance.

s/D_{helix}	s/D_{shaft}	$s(m)$	F_{ult} (kN)	n
1.10	5.5	1.10	499.6	0.956
1.20	6.0	1.20	497.3	0.952
1.40	7.0	1.40	497.2	0.952
1.60	8.0	1.60	501.6	0.960
2.00	10.0	2.00	518.7	0.993

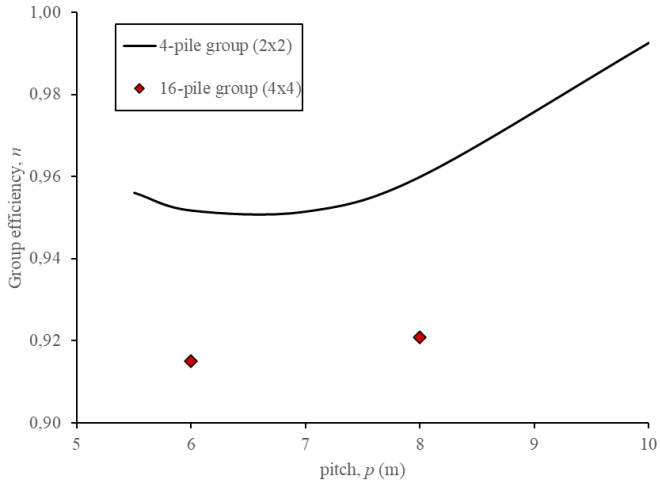

Figure 5. Effect of axial distance on the uplift capacity of a 4 pile group.

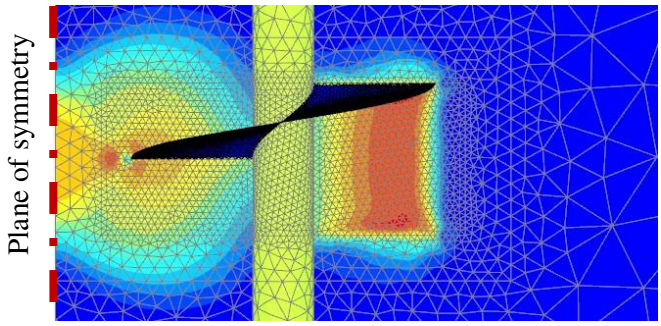

Figure 6. Incremental displacements at failure for 4-pile group with s/D_{helix} = 1.2.

5.2 *Group of 16 helical piles*

Two analyses were performed for a 16-pile group with a 4x4 layout and normalised spacings of s/D_{helix}=1.2 and 1.6 (s/D_{shaft}=6 and 8). As seen in Figure 5, group effects appear, as expected, to also depend on the number of piles in a helical pile group. The calculated group efficiencies for the above two pile spacings are as low as 0.915, which means that group effects are almost two times greater than those for a 4-pile group. Figure 7 shows a more extensive overlapping of the individual helix mechanisms compared to Figure 6, which explains the greater group effects in the case of a 16-pile group.

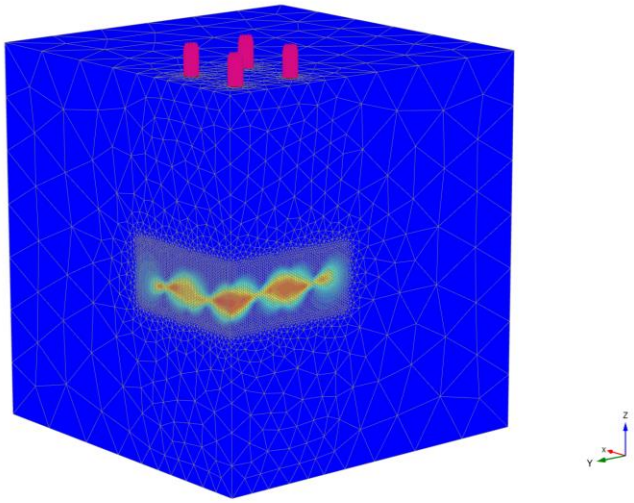

Figure 7. Incremental displacements at failure for 16-pile group with s/D_{helix} = 1.2.

6 CONCLUSIONS

Finite element analyses of axially loaded helical piles, individual helices and helical pile groups were presented. Simple geometrical approximations of helices, such as circular zero-thickness plates and circular tapered plates were first modelled and the calculated uplift capacities were shown to be in good agreement with published analytical and numerical solutions. The effect of the geometry of the helix was subsequently investigated. Finally, analyses of 4-pile and 16-pile helical pile groups were presented, and group effects were examined. The main conclusions of the study are summarised below:

- The failure mechanisms that develop in the soil when helices and helical piles are loaded axially to failure are non-symmetrical.
- The simplification of the helix geometry as a zero-thickness plate may result in overestimation of the uplift capacity on the order of 9%. The tapered plate approximation yields better results.
- As expected, the uplift capacity of a helical pile with a rough helix (full adhesion) is greater than that of a

helical pile with a smooth helix (zero adhesion). However, the effect of adhesion is smaller than that observed in plates.

- Group effects in the case of the two helical pile group layouts examined in this study depend on the pile spacing and the number of the piles. In all cases, the reduction of the total uplift capacity due to group effects was less than 10%.

7 REFERENCES

Byrne, B.W., Houlsby, G.T. 2015. Helical piles: an innovative foundation design option for offshore wind turbine foundations, *Philosophical Transactions A* **373(2035)**, 20140081.

Castro-Santos, L. Diaz-Casas, V. 2016. *Floating offshore wind farms*, Springer Cham, Switzerland.

Elsherbiny, Z.H., El Naggar, M.H. 2013. Axial compressive capacity of helical piles from field tests and numerical study, *Canadian Geotechnical Journal* **50(12)**, 1191–1203.

Houlsby, G. 2016. Interactions in offshore foundation design, *Géotechnique* **66(10)**, 791–825.

Lanyi-Bennett, S.A. Deng, L. 2017. Axial load testing of helical pile groups in glaciolacustrine clay. *Canadian Geotechnical Journal* **56(2),** 187-197.

Martin, C.M., Randolph, M.F. 2001. Application of the lower and upper bound theorems of plasticity to collapse of circular foundations. *10th Int. Conf. of the International Association for Computer Methods and Advances in Geomechanics* (C. Desai, T. Kundu, S. Harpalani, D. Contractor, J. Kemeny), 1417–1428. CRC Press, USA.

Merifield, R.S. 2011. Ultimate Uplift Capacity of Multiplate Helical Type Anchors in Clay, *Journal of Geotechnical and Geoenvironmental Engineering* **137(7)**, 704-716.

Merifield, R.S., Lyamin, A.V. Sloan, S.W. Yu, H.S. 2003. Three-Dimensional Lower Bound Solutions for Stability of Plate Anchors in Clay. *Journal of Geotechnical and Geoenvironmental Engineering* **129(3)**, 243-253

Perko, H.A. 1995. *Helical piles: A practical guide to design and installation*, John Wiley & Sons, Inc., USA.

Spagnoli, G. 2013. Some considerations regarding using helical piles as foundations for offshore structures. *Soil Mechanics and Foundation Engineering* **50(3)**, 102-110.

Ullah, S.N., Hu, Y., O'Loughlin, C. 2019. A Green Foundation for Offshore Wind Energy - Helical Piles. *World Engineers Convention, WEC2019* (P. Godfrey, D. Hargreaves, M. Kanga), 272-285. Engineers Australia, Australia.

Zhao, X., Randolph, M.F., Wang, D., Gaudin, C. 2015. Upper bound analysis of uplift capacity of a tapered plate anchor in cohesive soil, *Géotechnique Letters* **5,** 205-211.